HOKKAIDO UNIVERSITY

Title	Avoidance of four-wave mixing in optical fiber bundle for coherent anti-Stokes Raman scattering endomicroscopy
Author(s)	Ogawa, Hiroki; Hashimoto, Mamoru
Citation	Optics Letters, 46(14), 3356-3359 https://doi.org/10.1364/OL.425644
Issue Date	2021-07-06
Doc URL	http://hdl.handle.net/2115/86215
Rights	©2021 Optical Society of America. One print or electronic copy may be made for personal use only. Systematic reproduction and distribution, duplication of any material in this paper for a fee or for commercial purposes, or modifications of the content of this paper are prohibited
Type	article (author version)
File Information	FWM-supp-Ogawa.pdf

Instructions for use

Hokkaido University Collection of Scholarly and Academic Papers : HUSCAP

Avoidance of four-wave mixing in optical fiber bundle for coherent anti-Stokes Raman scattering endomicroscopy

HIROKI OGAWA[1] AND MAMORU HASHIMOTO[2*]

[1] Graduate School of Information Science and Technology, Hokkaido University, Kita 14, Nishi 9, Kitaku, Sapporo, Hokkaido, 060-0814, JAPAN
[2] Faculty of Information Science and Technology, Hokkaido University, Kita 14, Nishi 9, Kitaku, Sapporo, Hokkaido, 060-0814, JAPAN
[*] Corresponding author: hashimoto@ist.hokudai.ac.jp

Compiled July 15, 2021

We propose and demonstrate a method of suppressing four-wave mixing (FWM) in an optical fiber bundle to realize coherent anti-Stokes Raman scattering (CARS) endomicroscopy, which is the leading candidate for a definitive diagnosis of gastrointestinal cancer. Two excitation laser beams with different wavelengths are delivered via different cores to suppress FWM and are then combined with a polarization prism and a dual-wavelength waveplate and are focused to a spot. The background emission from the optical fiber bundle was suppressed to 1/3,289, and we demonstrated CARS imaging of a polystyrene bead using the proposed method. © 2021 Optical Society of America

http://dx.doi.org/10.1364/ao.XX.XXXXXX

In recent years, probe-based confocal laser scanning endoscopy (pCLE) has been developed to enable a definitive diagnosis of cancer by gastrointestinal endoscopy[1, 2]. Gastrointestinal endoscopy is widely used for early cancer diagnosis, but endoscopy alone cannot make a definitive diagnosis without a biopsy. pCLE overcomes this problem and provides cell morphology images comparable to pathological biopsy images[3–5]. pCLE uses a small-diameter microendoscope that approaches the affected area via an accessory channel in a gastrointestinal endoscope. By intravenously injecting a fluorescent dye such as fluorescein, pCLE provides cell images directly with 1000× magnification. As a result, a definitive diagnosis of cancer is no longer impossible. Still, the problem of the safety of intravenous fluorescein remains[6, 7].

Use of Raman scattering, which utilizes molecular vibrations to distinguish between molecular species and molecular states, solves the problems caused by staining. In vivo spontaneous Raman endoscopic probes for identifying cancerous tissue have been reported[8–10]. Raman probes have successfully diagnosed cancer by endoscopy with 97.0% sensitivity and 95.2% specificity. One problem, however, is that the spontaneous Raman scattering signal is weak. As a result, imaging takes time, and only the spectrum at a specific point is observed. Pathologists must diagnose cancer from the Raman spectra, which is a task that has not been familiar to them.

Endomicroscopy using coherent Raman scattering (CRS), such as coherent anti-Stokes Raman scattering (CARS) [11, 12] and stimulated Raman scattering (SRS) [13, 14], have been reported [15–23]. CARS and SRS provide 10^7 times higher efficiency than spontaneous Raman scattering [24] and can achieve imaging at video frame rates[25–28]. Furthermore, it is known that CRS provides clear shape images of the cell nucleus, which pathologists use to make pathological diagnoses, without staining[29]. However, no miniaturized CRS endoscope that can be inserted into the accessory channel of gastrointestinal endoscopes has been developed.

One of the problems that hinder the miniaturization of endoscopes is the generation of four-wave mixing (FWM) in an optical fiber. A probe-based endoscope that can pass through the accessory channel of a flexible gastrointestinal endoscope must have a small diameter and short rigid probe head. Since endoscopes that use optical fiber bundles do not require a beam scanning mechanism in the probe head, they are easy to miniaturize. On the other hand, CARS has advantages over SRS for endoscopes that detect light scattered backward. Therefore, we believe that a combination of an optical fiber bundle and CARS is suitable for label-free microendoscopy. However, with a combination of an optical fiber bundle and CARS, FWM occurs in the optical fiber[18, 30, 31]. The FWM wavelength is the same as that of CARS. We consider that the phase matching condition of FWM is not satisfied in the optical fiber, while its intensity is large compared with CARS because of the considerable length of the optical fiber.

In this letter, we propose a new method of suppressing FWM in a fiber bundle by using two excitation beams coupled into separate cores and superimposed at the probe head. Since FWM occurs when two excitation beams of different colors propagate through the same optical fiber core, FWM will be suppressed by transmitting the two beams through different cores. In addition, the excitation beams delivered by the individual cores are coaxially superposed by using the light polarization.

Figure 1 shows the principle of the proposed method. We use an optical fiber bundle with regularly aligned cores (Fig. 1(a)). The optical fiber bundle consists of thousands of

cores and cladding, and only the cores carry light. Therefore, when a laser beam is focused on the bundle end and scanned, the beam is delivered intermittently. Regularly arranged cores can deliver two light beams simultaneously, even if the beams are scanned. Figure 1 (b) shows that each beam is focused on different cores by adjusting the propagation angle. Figure 1 (c) shows that two excitation laser beams from different cores are superimposed by a polarizing prism such as a Wollaston prism or a Nomalski prism. The polarizing prism deflects both beams with their polarizations and superimposes the two beams coaxially. Of course, the distance d between the cores used for delivering, the focal length f of the collimation lens, and the separation angle θ of the polarizing prism must satisfy

$$d = f \tan(\theta). \quad \textbf{(1)}$$

In addition, since the polarizations of the two beams need to be aligned with the axis of the polarization prism, the polarization states incident on the bundle fiber must be adjusted. Since the polarization states of the two beams superimposed collinearly are orthogonal, the CARS efficiency is low. Therefore, a dual-wavelength waveplate is used to convert orthogonally polarized light beams into parallel polarized light beams that oscillate in the same direction. Here, the retardation of the dual-wavelength waveplate is 0 for the ω_p beam and π for the ω_s beam. The dual-wavelength waveplate does not interact with the ω_p beam, but it rotates the polarization of the ω_s beam. The proposed method results in a smaller field of view compared with the same core delivery. However, the affection is the beam separation distance and is a reduction of only a few percent.

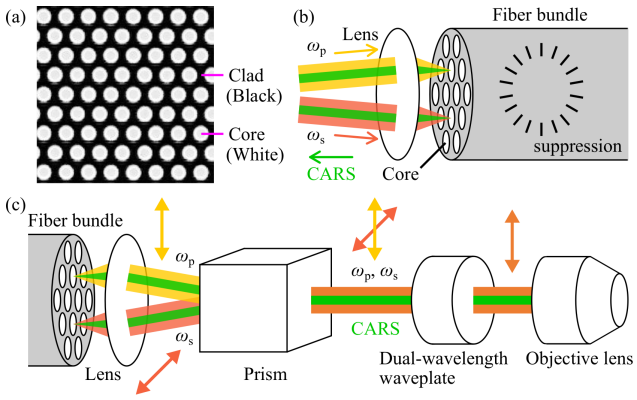

Fig. 1. Principle of the proposed method. (a) Optical fiber bundle with hexagonal close packing structure. White and black regions indicate cores and clad, respectively. (b) Schematic diagram of the proposed method at the entrance side of the fiber bundle. Two excitation laser beams (ω_p and ω_s) are coupled into separate cores. (c) Optical layout of endoscope head.

The experimental setup of the developed CARS imaging system is shown in Fig. 2. A picosecond mode-locked Ti:sapphire laser (repetition rate = 80 MHz, pulse duration = 5.48 ps, Tsunami, Spectra-Physics) was used for the pump beam. A picosecond acousto-optic tunable filter (AOTF) mode-locked Ti:sapphire laser (repetition rate = 80 MHz, pulse duration = 7.20 ps, Megaopt) was used for the Stokes beam[32]. The pump and Stokes wavelengths were tuned to 709 nm and 888 nm, respectively, to excite the CH_2 symmetric stretching vibration (2845 cm^{-1}). A synchronization system[33] tuned the temporal overlap, and an optical delay (SGSP26-200, Sigmakoki) provided a temporal time difference. The pump beam was adjusted to a polarization state orthogonal to the Stokes beam by a half-waveplate (HWP; AHWP05M-600, Thorlabs). The pump and Stokes beams were coupled into separate cores in an image fiber bundle (core diameter = 5.8 μm, pitch = 8.3 μm, length = 1.24 m, Sumita Optical Glass) using a 10× objective lens (CFI Plan Apo Lamda 10x, NA=0.45, Nikon) for delivery to the other end of the fiber bundle. After passing through the fiber bundle, the two beams were collimated by a 60× objective lens (LCPlanFI 60x, NA=0.7, Olympus), relayed by two achromatic lenses, and then collinearly superimposed by a Wollaston prism (Prism; WPQ10, Thorlabs). The orthogonal polarization states were converted to parallel polarization states with a customized dual-wavelength waveplate (Kougakugiken) to increase the excitation efficiency. The dual-wavelength waveplate behaved as a λ waveplate for the pump beam and a $\lambda/2$ waveplate for the Stokes beam. An objective lens (OL: UPlan Apo 40x, NA=0.85, Olympus) was used for imaging. The backscattered CARS signal was collected with the same objective lens and passed again through the fiber bundle. The dual-wavelength waveplate disturbs the polarization of CARS emission, while the polarizing prism divides CARS into orthogonal polarization components and lead to the cores to which the two excitation lights are delivered in opposite directions. Subsequently, the CARS signal was separated with a dichroic mirror (DM: FF660-Di02-25x36, Semrock), filtered with optical filters (F: FF01-609/54-25, FF01-591/6-25, FF01-680/SP-25, Semrock; 3rd560-640, Omega; FESH0650, Thorlabs), and detected with a photomultiplier tube (PMT: C9110, Hamamatsu). Transmitted light was also detected with a silicon photodiode (PD). The coupling efficiencies of the pump and Stokes beams were 57% and 47%, respectively. When two beams were coupling to the center of a core, coupling between neighbouring cores was rarely observed.

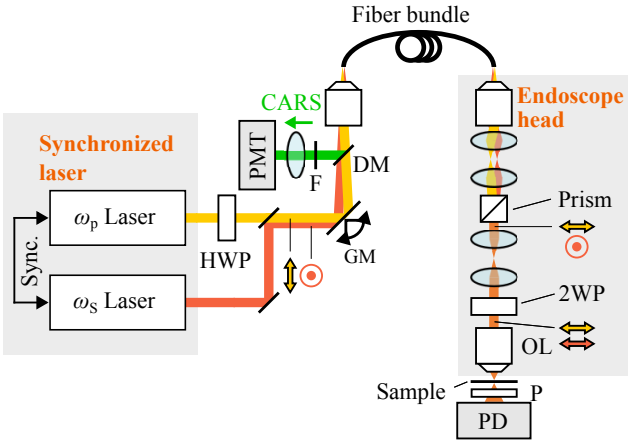

Fig. 2. Experimental setup of CARS imaging using optical fiber bundle. Sync: Synchronization system, HWP: Half-wave plate, GS: Galvanometer scanner, DM: Dichroic mirror, OL: Objective lens, Prism: Wollaston prism, 2WP: Dual-wavelength waveplate, P: Polarizer, PD: Photodiode, F: Filter, PMT: Photomultiplier tube.

Figure 3 shows the experimental results of suppressing FWM. We compared the emission from the optical fiber bundle when the two excitation beams were coupled into the same core (a, c) and separate cores (b, d)). Figures 3 (a) and (b) show the light output from the end face of the optical fiber bundle with-

out scanning of the beams. The emission from one core (a) and two cores (b) can be seen. Here, the images were observed with a CMOS camera by replacing the lens and the prism shown in Fig. 2. Figures 3 (c) and (d) show emission from the bundle with scanning of the beams and detecting the emitted light with the PMT. The high-intensity emission shown in Fig. 3 (c) was detected only when the two laser beams overlapped temporally. On the other hand, the emission shown in Fig. 3 (d) was greatly suppressed by delivering the two beams via separate cores, and its intensity was 1/3,289 of that in (c). We believe that the low emissivity was due to fluorescence and anti-Stokes Raman scattering from the fiber bundle because it appeared with the ω_p beam alone.

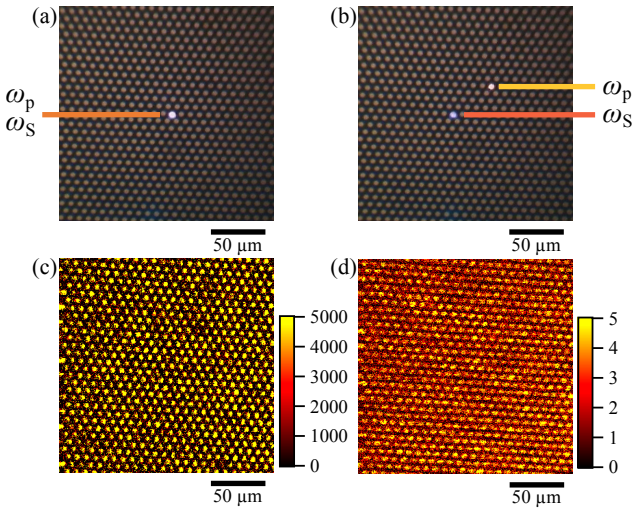

Fig. 3. Evaluation of the FWM suppression effect. Images of the light beams delivered via the optical fiber bundle when the two beams were coupled into the same core (a) and separate cores (b). The scanning of the laser beams was stopped. Image of emission from fiber bundle by scanning the laser beams when the two beams were coupled into the same core (c) and separate cores (d). The color scale in (d) is 1,000 times smaller than that in (c).

We observed CARS imaging by delivering two excitation beams via separate cores. Figure 4 shows transmission images (a-c) and CARS images (d-f) of a polystyrene bead with a diameter of 25 micrometers. In Figs. 4 (a, d), the polystyrene bead is present in the field of view, whereas in (b, e), the sample was moved, and the images do not include the bead. Here, the transmission images and the CARS images were acquired simultaneously. In the transmission image (a), the shadow of the polystyrene bead is clearly observed, and in the difference image (c = a−b), a more high contrast image is obtained. The low signals of two cores in Fig. 4b reflect fiber breakage of defects. The signal below the shadow of the polystyrene bead in Fig. 4c appears due to polarization disturbance during delivery in the fibers but does not contribute to CARS imaging. The CARS image (d) is not clear due to the background light (e) from the optical fiber, but the difference image (f = d−e) shows that a CARS image from the bead is obtained. However, when the two excitation beams were delivered via the same core, a CARS image could not be observed because the four-wave mixing was more than 3,000 times larger (see Fig. S1). The excitation light intensities on the sample surface were 41.5 mW (ω_p) and 2.5 mW (ω_s), the image size was 76 μm ×76 μm (250×250 pixels), and the image was observed at a rate of 300 s/image. The CARS images were smoothed with a 5 × 5 Gaussian filter. This subtraction technique is not a significant problem if we get an image without samples beforehand and subtract that image from an image with samples successively. Further experiments are required to demonstrate chemical specificity by comparing on-resonance and off-resonance images and improve spatial resolution for fine structure imaging. Although the dual-wavelength waveplate limits the observable spectral region, several tens cm^{-1} spectroscopic measurement will be available in the high Raman shift region.

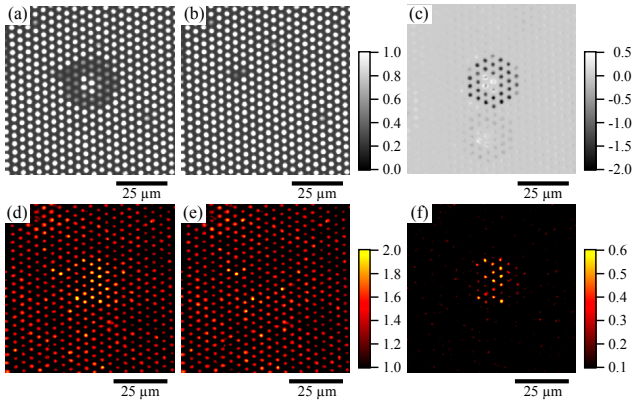

Fig. 4. Transmission (a, b) and CARS (d, e) images of a polystyrene bead and their subtracted images (c = a−b, f = d−e).

In the future, the CARS imaging system should be miniaturized to allow it to be inserted into the accessory channel of a gastrointestinal endoscope. In the proposed method, all optical elements were composed of transmissive elements and were coaxially arranged. The head size could be easily reduced by using a refractive index (GRIN) lens and a small prism that combines a polarizing prism and a dual-wavelength waveplate. For example, by using commercially available GRIN lenses with a diameter of 2 mm for the fiber collimator (10 mm length) and the objective lens (5 mm length) , and a small prism with a diameter of 2 mm and a length of 3.2–5.2 mm, the head size could be reduced to have a diameter of 2 mm and a total length of about 20 mm, which would allow it to be inserted into the accessory channel.

In conclusion, we proposed a method of suppressing the generation of FWM in a fiber bundle to realize CARS microendoscopic imaging. The proposed method has the following features:

1) Two excitation beams in orthogonally polarized states are coupled and delivered via different cores in a fiber bundle in which the cores are regularly aligned.
2) In the head part, a polarizing prism coaxially superimposes the two excitation beams delivered by different cores.
3) A dual-wavelength waveplate converts the orthogonal polarizations of the two excitation beams to parallel polarizations.

We also designed and constructed a CARS imaging system to demonstrate the proposed method, and we quantitatively evaluated the FWM suppression effect. As a result, the FWM intensity generated by the optical fiber was suppressed to 1/3,289. The usefulness of the proposed method was confirmed by demonstrating CARS imaging of 25 μm polystyrene beads with suppression of FWM in the optical fibers. From our

results, we believe that our method will significantly contribute to achieving a definitive diagnosis during endoscopic inspection using CARS microendoscopy.

Funding.

Research granted from The Murata Science Foundation.

Disclosures.

The authors declare no conflicts of interest.

Supplemental document

See Supplement 1 for supporting content.

REFERENCES

1. J. Wang, M. Yang, L. Yang, Y. Zhang, J. Yuan, Q. Liu, X. Hou, and L. Fu, Engineering **1**, 351–360 (2015).
2. S. S. Chauhan, B. K. A. Dayyeh, Y. M. Bhat, K. T. Gottlieb, J. H. Hwang, S. Komanduri, V. Konda, S. K. Lo, M. A. Manfredi, J. T. Maple, F. M. Murad, U. D. Siddiqui, S. Banerjee, and M. B. Wallace, Gastrointest. Endosc. **80**, 928–938 (2014).
3. G. H. Bok, S. R. Jeon, J. Y. Cho, J.-H. Cho, W. C. Lee, S. Y. Jin, I. H. Choi, H. G. Kim, T. H. Lee, and E. J. Park, Gastrointest. Endosc. **77**, 899–908 (2013).
4. M. I. Canto, S. Anandasabapathy, W. Brugge, G. W. Falk, K. B. Dunbar, Z. Zhang, K. Woods, J. A. Almario, U. Schell, J. Goldblum, A. Maitra, E. Montgomery, R. Kiesslich, and Confocal Endomicroscopy for Barrett's Esophagus or Confocal Endomicroscopy for Barrett's Esophagus (CEBE) Trial Group, Gastrointest. Endosc. **79**, 211–221 (2014).
5. N. Horiguchi, T. Tahara, H. Yamada, D. Yoshida, M. Okubo, M. Nagasaka, Y. Nakagawa, T. Shibata, T. Tsukamoto, M. Kuroda, and N. Ohmiya, Dig. Endosc. **30**, 219–227 (2018).
6. M. Wallace, A. Meining, M. Canto, P. Fockens, S. Miehlke, T. Roesch, C. Lightdale, H. Pohl, D. Carr-Locke, M. Löhr *et al.*, Aliment. Pharmacol. & Ther. **31**, 548–552 (2010).
7. L. A. Yannuzzi, K. T. Rohrer, L. J. Tindel, R. S. Sobel, M. A. Costanza, W. Shields, and E. Zang, Ophthalmology **93**, 611–617 (1986).
8. M. Bergholt, W. Zheng, K. Lin, K. Ho, M. Teh, K. Yeoh, J. Y. So, and Z. Huang, Technol. Cancer Res. & Treat. **10**, 103–112 (2011).
9. M. S. Bergholt, W. Zheng, K. Y. Ho, K. Yeoh, and Z. Huang, J. Gastroint. Dig. Syst. S **1**, 008 (2013).
10. M. S. Bergholt, W. Zheng, K. Y. Ho, M. Teh, K. G. Yeoh, J. B. Y. So, A. Shabbir, and Z. Huang, Gastroenterology **146**, 27–32 (2014).
11. A. Zumbusch, G. R. Holtom, and X. S. Xie, Phys. Rev. Lett. **82**, 4142 (1999).
12. M. Hashimoto, T. Araki, and S. Kawata, Opt. Lett. **25**, 1768–1770 (2000).
13. C. W. Freudiger, W. Min, B. G. Saar, S. Lu, G. R. Holtom, C. He, J. C. Tsai, J. X. Kang, and X. S. Xie, Science **322**, 1857–1861 (2008).
14. Y. Ozeki, F. Dake, S. Kajiyama, K. Fukui, and K. Itoh, Opt. Express **17**, 3651–3658 (2009).
15. B. G. Saar, R. S. Johnston, C. W. Freudiger, X. S. Xie, and E. J. Seibel, Opt. Lett. **36**, 2396–2398 (2011).
16. F. Légaré, C. L. Evans, F. Ganikhanov, and X. S. Xie, Opt. Express **14**, 4427–4432 (2006).
17. A. Lombardini, V. Mytskaniuk, S. Sivankutty, E. R. Andresen, X. Chen, J. Wenger, M. Fabert, N. Joly, F. Louradour, A. Kudlinski, and H. Rigneault, Light. Sci. & Appl. **7**, 1–8 (2018).
18. A. Lukic, S. Dochow, H. Bae, G. Matz, I. Latka, B. Messerschmidt, M. Schmitt, and J. Popp, Optica **4**, 496–501 (2017).
19. K. Hirose, T. Aoki, T. Furukawa, S. Fukushima, H. Niioka, S. Deguchi, and M. Hashimoto, Biomed. Opt. Express **9**, 387–396 (2018).
20. M. Balu, G. Liu, Z. Chen, B. J. Tromberg, and E. O. Potma, Opt. Express **18**, 2380–2388 (2010).
21. K. Hirose, S. Fukushima, T. Furukawa, H. Niioka, and M. Hashimoto, APL Photonics **3**, 092407 (2018).
22. C.-S. Liao, P. Wang, C. Y. Huang, P. Lin, G. Eakins, R. T. Bentley, R. Liang, and J.-X. Cheng, ACS Photonics **5**, 947–954 (2017).
23. P. Zirak, G. Matz, B. Messerschmidt, T. Meyer, M. Schmitt, J. Popp, O. Uckermann, R. Galli, M. Kirsch, M. Winterhalder *et al.*, APL Photonics **3**, 092409 (2018).
24. H. Rigneault and P. Berto, APL Photonics **3**, 091101 (2018).
25. C. L. Evans, E. O. Potma, M. Puoris' haag, D. Côté, C. P. Lin, and X. S. Xie, Proc. Natl. Acad. Sci. **102**, 16807–16812 (2005).
26. T. Minamikawa, M. Hashimoto, K. Fujita, S. Kawata, and T. Araki, Opt. Express **17**, 9526–9536 (2009).
27. B. G. Saar, C. W. Freudiger, J. Reichman, C. M. Stanley, G. R. Holtom, and X. S. Xie, Science **330**, 1368–1370 (2010).
28. Y. Ozeki, W. Umemura, Y. Otsuka, S. Satoh, H. Hashimoto, K. Sumimura, N. Nishizawa, K. Fukui, and K. Itoh, Nat. Photonics **6**, 845–851 (2012).
29. S. Weng, X. Xu, J. Li, and S. T. C. Wong, J. Biomed. Opt. **22**, 1 – 10 (2017).
30. A. Lukić, S. Dochow, O. Chernavskaia, I. Latka, C. Matthäus, A. Schwuchow, M. Schmitt, and J. Popp, J. Biophotonics **9**, 138–143 (2016).
31. Z. Wang, L. Gao, P. Luo, Y. Yang, A. A. Hammoudi, K. K. Wong, and S. T. Wong, Opt. Express **19**, 7960–7970 (2011).
32. H. Cahyadi, J. Iwatsuka, T. Minamikawa, H. Niioka, T. Araki, and M. Hashimoto, J. Biomed. Opt. **18**, 096009 (2013).
33. T. Minamikawa, N. Tanimoto, M. Hashimoto, T. Araki, M. Kobayashi, K. Fujita, and S. Kawata, Appl. Phys. Lett. **89**, 191101 (2006).